

3D Modelling and Study of Electrochemical Characteristics and Thermal Stability of Commercial Accumulator by Simulation Methods

P. Vyroubal¹, T. Kazda^{1,*}, J. Maxa¹, J. Vondrák¹, M. Sedlaříková¹, J. Tichý¹ and R. Cipín²

¹ Department of Electrical and Electronic Technology, Faculty of Electrical Engineering and Communication, BUT, Technická 10, 616 00 Brno, Czech Republic

² Department of Power Electrical and Electronic Engineering, Faculty of Electrical Engineering and Communication, BUT, Technická 10, 616 00 Brno, Czech Republic

*E-mail: tomaskazda@volny.cz

Received: 22 November 2015 / *Accepted:* 31 December 2015 / *Published:* 1 February 2016

Lithium-ion batteries are one of the most expanding types of batteries on the market these days. They are widely used in recent years not only in portable devices but also increasingly in the automotive industry (BMW i3, Tesla S) or in aerospace (Boeing 787, Lockheed F-35) because of their very high capacity and energy density. Demands on safety of these batteries grow with their use in more and more devices. Safety is an important issue particularly in the case of Li-Ion batteries because of the large amount of energy stored inside them and also because of their great sensitivity to the conditions in which these batteries are used. One possibility to verify the battery behaviour under different conditions (current load, temperature), is the creation of a physical-mathematical model of the battery and by using the simulation to predict its behaviour. These methods can save time when we test batteries in a real device such as in a car for example. It is equally possible to set up a model of the real battery and implement parameters of a new type of electrode material which is tested only in the laboratory into the model. Then we can, thanks to the simulation, predict the behaviour of the battery with this advanced material. Compilation of the physical-mathematical model of a real battery and verification of the model by using electrochemical testing of a real battery are discussed in this article. The real battery was discharged by different currents and its discharge characteristics were measured by a potentiostat. At the same time, this cell was scanned with a thermographic camera in order to verify its heating. Discharge characteristics and battery heating were subsequently simulated by using a physical-mathematical model. Deviations between the simulation and the measurement results obtained during heating by high current flow were very small - between 1 and 5 %.

Keywords: Lithium ion battery, numerical model, field, heating, simulations

1. INTRODUCTION

Li-Ion batteries are composed, like other batteries, from an anode, a cathode and a separator. The anode and cathode are made of compounds which allow intercalation and de-intercalation of lithium ions into their structure during cycling. The process of charging and discharging of the Li-Ion batteries is provided only by transition of lithium ions from anode to cathode and back. Therefore, there are not any complex electrochemical reactions that lead to the degeneration of the battery.[1-4] The main reason for the interest and development of lithium-ion batteries was a very high specific capacity of lithium - 3.86 Ah/g and a very high reduction potential of -3.045 V. The LiCoO₂ cathode material was discovered in 1980. It was subsequently commercially used as the first cathode material in 1990 by SONY in their batteries.[4] The main advantage of this material is its high theoretical capacity of 272 mAh/g and the high potential versus lithium - 3.88 V. The main disadvantages are: low temperature stability, lower real achievable capacity (only 145 mAh/g), the high cost, decrease of the potential and its capacity during discharging by high currents.[5][6] Temperature instability is one of the biggest problems of this material which has led for example to fire of batteries in Boeing 787 airplanes.[7] A more recent type of cathode material is LiMn₂O₄ which is characterized by spinel structure which makes them more stable than LiCoO₂ and by the high potential of the discharge plateau (4.1 V vs. Li). The disadvantage of this material is its lower achievable capacity 120 mAh/g and the tendency for progressive degeneration due to dissolution of manganese into the electrolyte during cycling. Another newer and more frequently used material is LiFePO₄ discovered in 1996. This material with olivine structure is characterized by high structural stability which makes its durability during cycling very high and it is also thermally very stable. Another advantage is its high practically achievable capacity about 160 mAh/g. The disadvantages of this material are its higher price and also lower potential vs. lithium (3.3 V). The newest type of cathode material is the LiNi_{0,33}Mn_{0,33}Co_{0,33}O₂ material which is characterized by high stability close to the stability of LiFePO₄. Other advantages are the high achievable capacity about 170 mAh/g and a high potential versus lithium of 3.7 V. Disadvantage of this cathode material is the greater cost due to the presence of precious metals.[5][6] The battery with this type of cathode material was also tested in this article.

2. MATHEMATICAL PHYSICAL MODEL

The issue of numerical modelling of lithium-ion batteries lies in the geometric model, where it is necessary to define each layer of the structures. These structures are sandwich type, very thin and moreover, they act in several layers, which implies a problematic formation of a computational mesh in 3D. Furthermore, these domains are of multiphysical character, i.e. the solution comprises the association of several types of properties (e.g. conductivity, heat capacity, thermal conductivity, mechanical properties, etc.), which greatly complicates the problem.

First, we used the classical model based on using porous electrode and concentrated solution theories. The model can accurately capture Li-ion migration in the battery. It schematically shows the electrode plate pair in the Li-ion battery (See fig. 1). The composite electrode consists of active

materials and electrolyte solution. The electrolyte phase is continuous across the negative electrode, separator and positive electrode while solid phase only exists in the negative and positive electrode. The solid active material is modelled as a matrix of mono-sized spherical particles.

The electrolyte in the modelled batteries has to be a quiescent binary 1:1 electrolyte, containing lithium cations (Li^+) and anions (An^-) (6). In the electrolyte and pore electrolyte, two variables (ϕ_1 and c_1) are defined. Assuming electroneutrality, c_1 denotes both the Li^+ concentration and the An^- concentration. Charge-conservation equations are solved for the electric potentials of the electrode and electrolyte phases throughout the cell. The domain equations in the electrolyte are the conservation of charge and the mass balance for the salt according to the following:

$$i_{\text{tot}} + Q_1 = \nabla \cdot \left(-\sigma_1 \nabla \phi_1 + \frac{2\sigma_1 RT}{F} \left(1 + \frac{\partial \ln f}{\partial \ln c_1} \right) (1 - t_+) \nabla \ln c_1 \right) \quad (1)$$

and

$$R_1 - \left(\frac{i_{\text{tot}} + Q_1}{F} \right) t_+ = \varepsilon_1 \frac{\partial c_1}{\partial t} + \nabla \cdot (-D_1 \nabla c_1) \quad (2)$$

where σ_1 denotes the electrolyte conductivity, f the activity coefficient for the salt, t_+ the transport number for Li^+ (also called transference number), i_{tot} the sum of all electrochemical current sources, and Q_1 denotes an arbitrary electrolyte current source. In the mass balance for the salt, ε_1 denotes the electrolyte volume fraction, D_1 the electrolyte salt diffusivity, and R_1 the total Li^+ source term in the electrolyte.

Equations (1) and (2) are spatially second order and thus each require boundary conditions. Fig. 1 summarizes the conservation equations and the boundary conditions illustrated in a one-dimensional configuration where the normal vector \mathbf{n} points into the electrolyte domain.

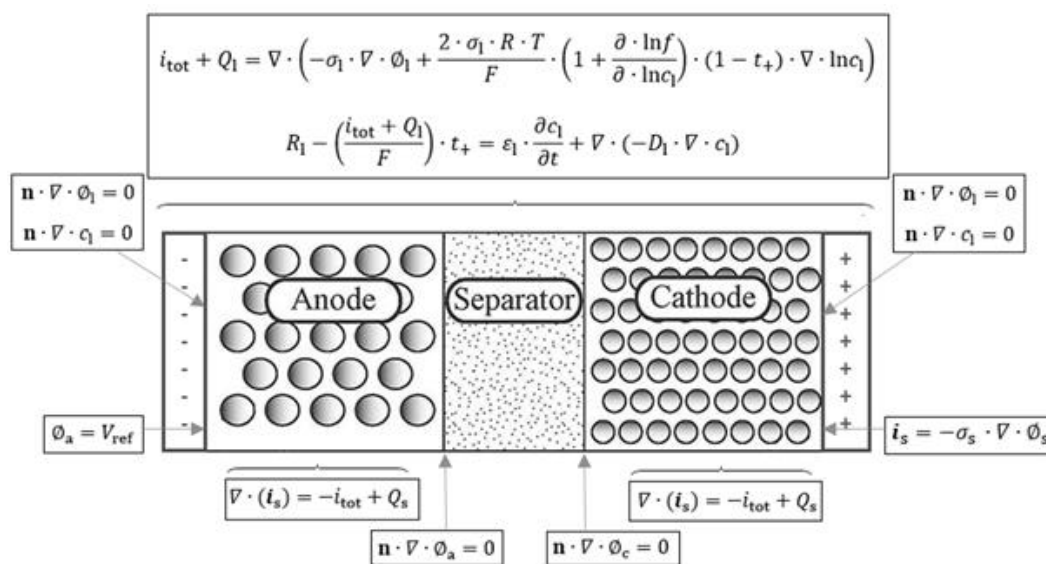


Figure 1. Schematic model of electrode plate pair in the Li-ion battery with boundary conditions illustrated in a one-dimensional configuration.[8]

In the porous electrodes, i_{tot} denotes the sum of all charge transfer current density contributions according to:

$$i_{tot} = \sum A_{v,m} i_{loc,m} \tag{3}$$

where $A_{v,m}$ represents the surface area of active electrode particles per unit volume of composite electrode. In the electrode, the current density, i_s is defined as:

$$i_s = -\sigma_s \nabla \phi_s \tag{4}$$

where σ_s is the electrical conductivity. The domain equation for the electrode is the conservation of charge expressed as:

$$\nabla \cdot (i_s) = -i_{tot} + Q_s \tag{5}$$

where Q_s is an arbitrary current source term. The first term in the equation (8) represents charge transport via electric conduction. The second term represents a source of charge associated with electrons entering (leaving) the solid electrode phase via charge-transfer reactions.

The electrochemical reactions in the physical interface are assumed to be insertion reactions occurring at the surface of small solid spherical particles of radius r_p in the electrodes. The insertion reaction is described as:



where Θ_s denotes a free reaction site and $Li\Theta_s$ an occupied reaction site at the solid particle surface. The concentration of Θ_s does not have to be solved for since the total concentration of reaction sites, $c_{s,max}$, is assumed to be constant, implying that:

$$c_{\Theta_s} = c_{s,max} - c_s \tag{7}$$

An important parameter for lithium insertion electrodes is the state-of-charge variable for the solid particles, denoted **SOC**. This is defined as:

$$SOC = \frac{c_s}{c_{s,max}} \tag{8}$$

The equilibrium potentials E_0 of lithium insertion electrode reactions are typically functions of **SOC**. The electrode reaction occurs on the particle surface and lithium diffuses to and from the surface in the particles. The mass balance of Li in the particles is described as:

$$\frac{\partial c_s}{\partial t} = \nabla \cdot (-D_s \nabla c_s) \tag{9}$$

where c_s is the concentration of **Li** in the solid phase. This equation is solved locally by the physics interface in a 1D pseudo dimension, with the solid phase concentrations at the nodal points for the element discretization of the particle as independent variables. The gradient is calculated in Cartesian, cylindrical or spherical coordinates, depending on the particles which are assumed to be the best for the description - flakes, rods or spheres, respectively.

A resistive film (also called solid-electrolyte interface, SEI) might form on the solid particles resulting in additional potential losses in the electrodes. To model the film resistance, an extra solution variable for the potential variation over the film, $\Delta\phi_{s,film}$ is introduced in the physical interface. The governing equation then accords to:

$$\Delta\phi_{s,film} = i_{tot} R_{film} \tag{10}$$

where R_{film} (Ω/m^2) denotes a generalized film resistance. The activation overpotentials, η_m , for all electrode reactions in the electrode then receive an extra potential contribution:

$$\eta_m = \phi_s - \Delta\phi_{s,film} - \phi_l - E_{eq,m} \tag{11}$$

The rate of a charge-transfer process is usually modelled with a Butler–Volmer equation, which can apply to an elementary or a global reaction. In Butler–Volmer form, the current density is evaluated as:

$$i = i_0 \cdot \left(\exp\left(\frac{\alpha_a F}{RT} \eta\right) - \exp\left(\frac{\alpha_c F}{RT} \eta\right) \right) \quad (12)$$

Second, we used the MSMD model (Multi-Scale Multi-Domain), which comprises different physical properties for each layer used. This MSMD model simulated the electrochemical behavior at the particle, electrode, and cell domains, with appropriate coupling between the scales. This allowed multiple cell designs to be tested, while only using a 1D model for the electrode domain (analogous to cell sandwich level), but being able to model the temperature in 3D. Thermal and electric field are calculated in the active core of the battery according to the following differential equations:

$$\frac{\partial \rho C_p T}{\partial t} - \nabla \cdot (k \nabla T) = q \quad (13)$$

resp.

$$\frac{\partial \rho C_p T}{\partial t} - \nabla \cdot (k \nabla T) = \sigma_+ |\nabla \Phi_+|^2 + \sigma_- |\nabla \Phi_-|^2 + \dot{q}_{ECh} + \dot{q}_{short} \quad (14)$$

and

$$\nabla \cdot (\sigma_+ \nabla \Phi_+) = -j \quad (15)$$

resp.

$$\nabla \cdot (\sigma_+ \nabla \Phi_+) = -(j_{ECh} - j_{short}) \quad (16)$$

and

$$\nabla \cdot (\sigma_+ \nabla \Phi_+) = j \quad (17)$$

resp.

$$\nabla \cdot (\sigma_- \nabla \Phi_-) = (j_{ECh} - j_{short}) \quad (18)$$

where σ_+ a σ_- are conductivities of positive and negative electrode, Φ_+ a Φ_- are potentials of positive and negative electrode, j_{ECh} a \dot{q}_{ECh} volumetric current and heat generated by electrochemical reactions, respective j_{short} a \dot{q}_{short} volumetric current and heat generated by internal short circuit (in normal conditions these variables are equal to zero). Electrochemical sub-models relate the local current density to the potential. Cell model couples sub-models to thermal and electrical fields within the cell, integrates over multiple electrode-pairs.

The internal model is calculated by means of the Newman, Tiedemann, Gu, and Kim model, which is simple semi-empirical electrochemical model. It was proposed by Kwon [9] and has been used by [10] and [11]. In the model formulation, the current transfer is related to the potential field by the following algebraic equation:

$$j = aY[U - (\Phi_+ - \Phi_-)] \quad (19)$$

where a is the specific area of the electrode sandwich sheet in the battery and U are the model parameters which are functions of the battery depth of discharge (DoD):

$$DoD = \frac{Volume}{3600 Q_{Ah}} \left(\int_0^t j dt \right) \quad (20)$$

where **Volume** denotes the battery volume, and Q_{Ah} is the battery total electric capacity in Ampere hours.

For a given battery, the voltage-current response curve can be obtained through experimentation;

Y and U can then be determined by curve fitting the data. The following formulation for the Y and U functions are:

$$Y = \sum_{n=0}^5 (a_n (DoD)^n) \exp \left[-C_1 \left(\frac{1}{T} - \frac{1}{T_{ref.}} \right) \right] \quad (21)$$

and

$$U = \sum_{n=0}^3 (b_n (DoD)^n) - C_2 (T - T_{ref.}) \quad (22)$$

where C_1 and C_2 are the the Newman, Tiedemann, Gu, and Kim model constants. The energy source term comes from the contribution of Joule heating, electrochemical reaction heating, and the entropic heating:

$$q = \sigma_+ |\nabla \phi_+|^2 + \sigma_- |\nabla \phi_-|^2 + j [U - (\phi_+ - \phi_-) - T \frac{dU}{dT}] \quad (23)$$

For calculation of effective values of material density, thermal conductivity and heat capacity, the following equations are used:

$$x_{eff} = \frac{0,5x_c^p \delta_c^p + x_e^p \delta_e^p + x_s \delta_s + x_e^n \delta_e^n + x_c^n \delta_c^n}{\delta_{total}} \quad (24)$$

$$\delta_{total} = 0,5\delta_c^p + \delta_e^p + \delta_s + \delta_e^n + 0,5\delta_c^n \quad (25)$$

where x_{eff} is the effective value of the given characterization of the material (density, heat capacity, thermal conductivity) and it is function of the material thickness. Indexes c, e and s denote current collector, electrode and separator and indexes p and n denote positive or negative electrode. δ_{total} is the total thickness of the specimen.

The simulation model accepts the Multi-scale physics from sub-micro-scale to battery-dimension-scales.

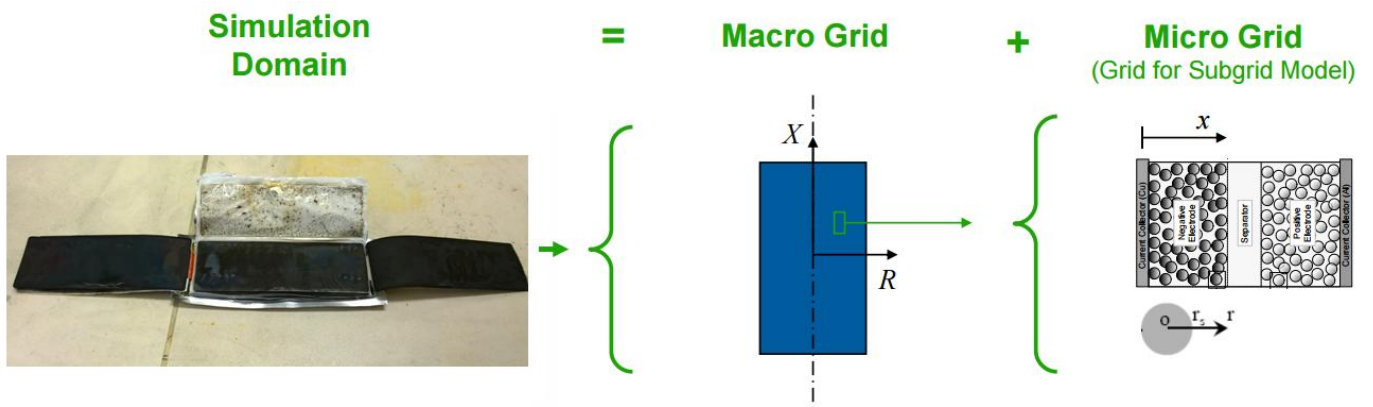


Figure 2. Dividing of the numerical model.

These equations are valid for electrical conductivity:

$$\sigma_p = \frac{0,5\sigma_c^p \delta_c^p + \sigma_e^p \delta_e^p}{\delta_{total}} \quad \text{and} \quad \sigma_n = \frac{0,5\sigma_c^n \delta_c^n + \sigma_e^n \delta_e^n}{\delta_{total}} \quad (26)$$

After the experimental measurement, the investigated battery was disassembled in order to obtain the geometrical dimensions. The global parameters of thermal conductivity, heat capacity, electrical conductivity, density and length parameters of the battery were determined from the above relationships (See TABLE I.).

Table I. Dimensions and properties of the battery.

| Zone | Pc | Pe | S | Ne | Nc | Total |
|-------------------------------|----------|----------|----------|----------|----------|-------------------|
| Delta [m] | 8,40E-04 | 2,44E-03 | 9,24E-04 | 4,28E-04 | 1,05E-04 | 8,52E-03 |
| Density [kg/m ³] | 2700 | 1500 | 492 | 2660 | 8900 | 8,04E+02 |
| Heat capacity [J/kg/K] | 903 | 1260 | 1978 | 1437 | 385 | 6,94E+02 |
| Thermal conductivity [W/m/K] | 238 | 1,48 | 0,334 | 1,04 | 398 | 1,47E+01 |
| Electrical conductivity [S/m] | 3,89E+07 | 1,00E-06 | | 1,00E+04 | 6,33E+07 | ρ_p 1,92E+06 |
| | | | | | | ρ_n 3,90E+05 |

A computational mesh with 49 259 elements and 23 689 nodes was used. An unstructured meshing method was used for better meshing process.

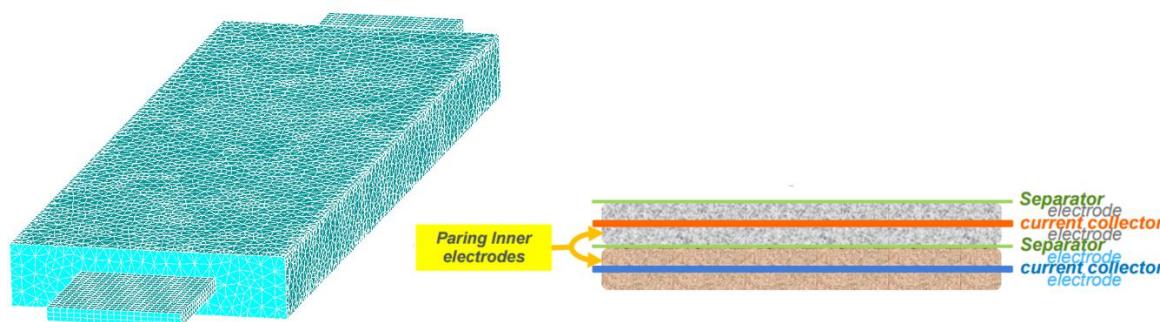


Figure 3. Computational mesh and the sandwich structure of the battery.

An unstructured grid is identified by irregular connectivity. It cannot easily be expressed as a two-dimensional or three-dimensional array in a computer memory. This allows for any possible element that a solver might be able to use. The time dependent analysis for discharge cycle was used.

3. EXPERIMENTAL

Two Li-Ion 4 Ah batteries model SLPB9543140H5 made by KOKAM company were used for electrochemical testing and preparation of physical-mathematical model. First battery was disassembled and the dimensions of its parts have been measured and used for the model preparation. The second battery was connected to the potentiostat Biologic Science Instruments® VMP3® with a booster. CCCV was always used as a battery charging method. The charging current was set to 0.2 C

(800 mA); cut-off voltage to 4.2 V. The potentiostat was switched to the CV mode upon reaching 4.2 V and charging continued until the current dropped below 200 mA. Subsequently, the tested battery was discharged by currents of 0.2 C (0.8 A), 0.5 C (2 A), 1 C (4 A), 2 C (8 A) and 4 C (16 A). Discharge characteristics were always recorded during discharging and the battery was continuously photographed by a thermographic camera to determine the heating of the battery when current passes through at high C rates (more than 1 C). The resulting discharge characteristics and battery temperature detected during discharging by the current higher than 1 C were compared with the results obtained by simulation.

4. RESULTS AND DISCUSSION

Fig. 4 shows the comparison of discharge curves with different C rate of the KOKAM battery. It can be seen that the battery maintains a very stable discharging plateau at 0.2 C and the profile of discharging plateau is the same for every tested C rate. The potential of discharge plateau decreases with increasing current load. However this decline is not too steep even at the highest loads. Capacity decline is also not very significant. Reached capacities are in the range between 3509 mAh and 3320 mAh which represents a capacity decrease of 5.4 %. It can be seen from these results that the tested battery behaved very stable at various stages of discharge and different loads.

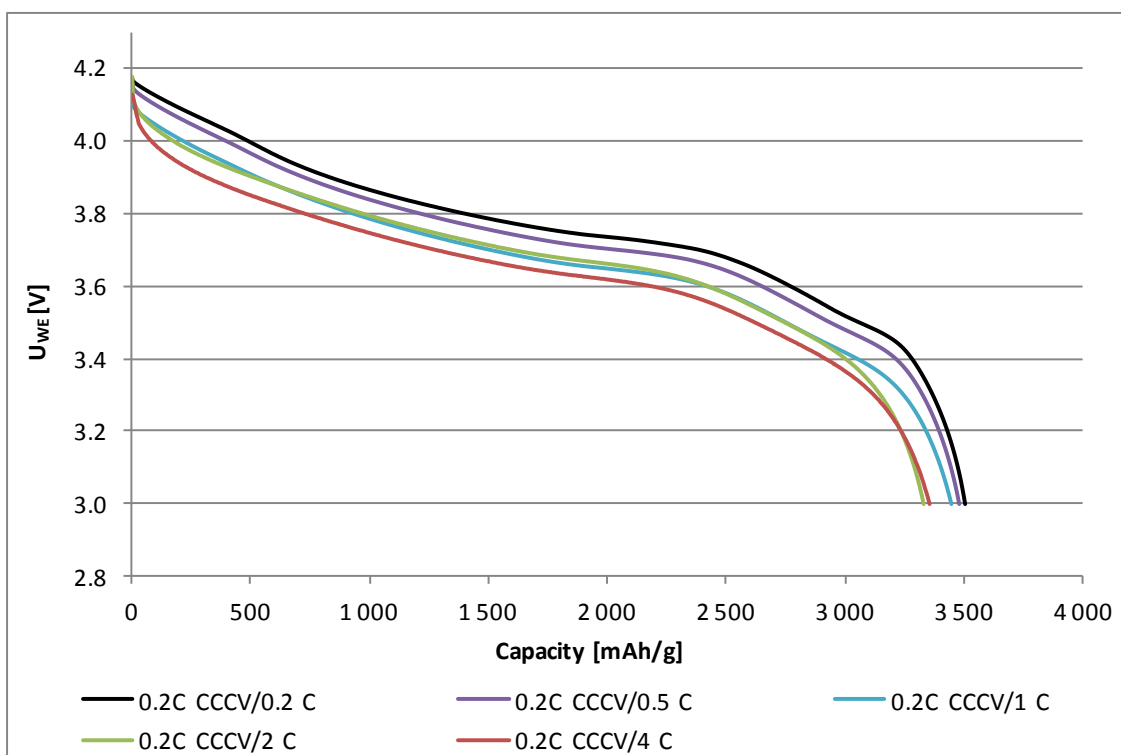


Figure 4. Comparison of discharge curves for real tested battery KOKAM for different C rates - 0.2 C (0.8 A), 0.5 C (2 A), 1 C (4 A), 2 C (8 A) and 4 C (16 A)

The observed decrease of capacity corresponds with the decrease of capacity specified in the technical specification of this model of battery.[12] However, the observed capacity is lower in comparison with the capacity declared by the manufacturer by almost 500 mAh. This deviation between the capacity reported by the producer and the real capacity occurs frequently and, in some cases, is very significant and exceeds 50% of the declared capacity. [13,14]

We can see a comparison of the real battery KOKAM and MSMD model for 1 C current in Fig. 5. It is evident from these curves that the simulated discharge potential was slightly higher than real measurement but the final reached capacity is practically the same as during the real measurement.

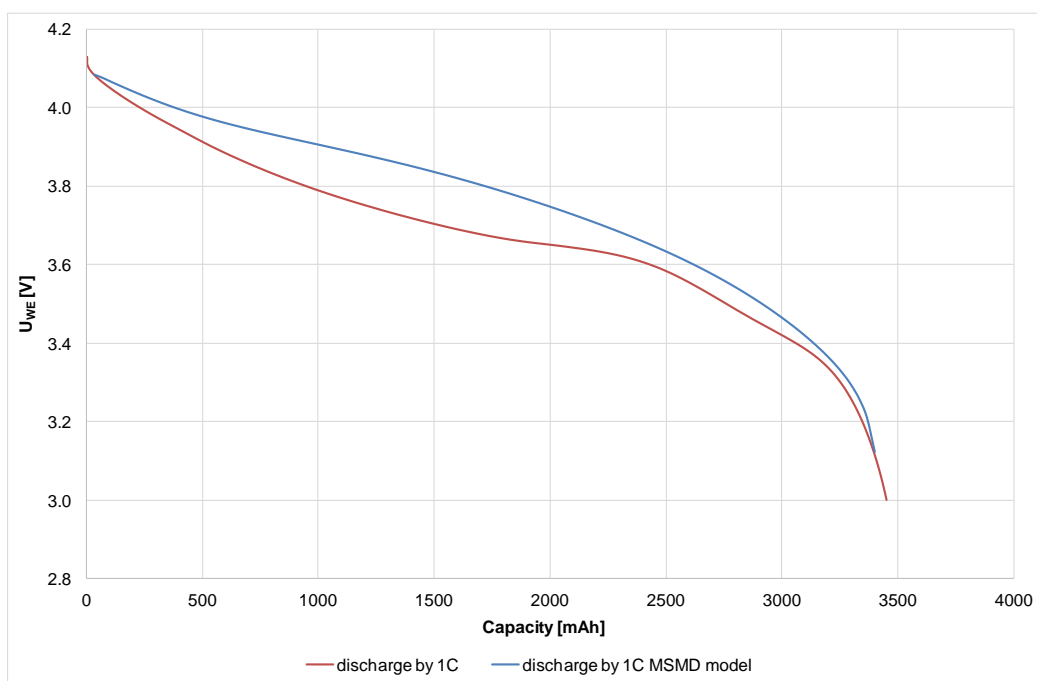


Figure 5. Comparison of the discharge curves for discharging at 1 C for the real KOKAM battery (red) and the mathematical physical model KOKAM (blue)

A comparison the real battery KOKAM and MSMD model at 2 C discharge current can be seen in Fig. 6. Discharge profile taken by the simulation is more similar to the discharge profile observed during the measurement when compared with the previous figure. The capacity obtained by simulation is higher than the real measured capacity. The difference between these capacities is 3.2 %. A comparison at 4 C discharge rate can be seen in Fig. 7. Discharge characteristics are practically identical but the capacity reached by simulation is again slightly higher. In this case, the difference of the achieved capacity is equal to 3.1 %. Observed deviations of the achieved capacities are very small - less than 5 % which were reported in another article at a discharge current 1 C. [15]

The result from monitoring the temperature distribution using the thermographic camera and the result from the simulation of distribution of thermal field during discharging by 1 C are both shown in Fig. 10. We can see that the simulated temperature distribution is practically identical as the one from the real measurement by the thermographic camera. We can see from the values of the maximum

temperatures achieved in the simulation and measurement, which are listed in Table 2, that in the case of measuring the maximum temperature reached 28.3 °C and 26.95 °C in the case of simulation. This difference equals to 4.7 %. Fig. 11 shows the temperature distribution obtained by using the thermographic camera and the result from the simulation of distribution of thermal field during discharging by 2 C.

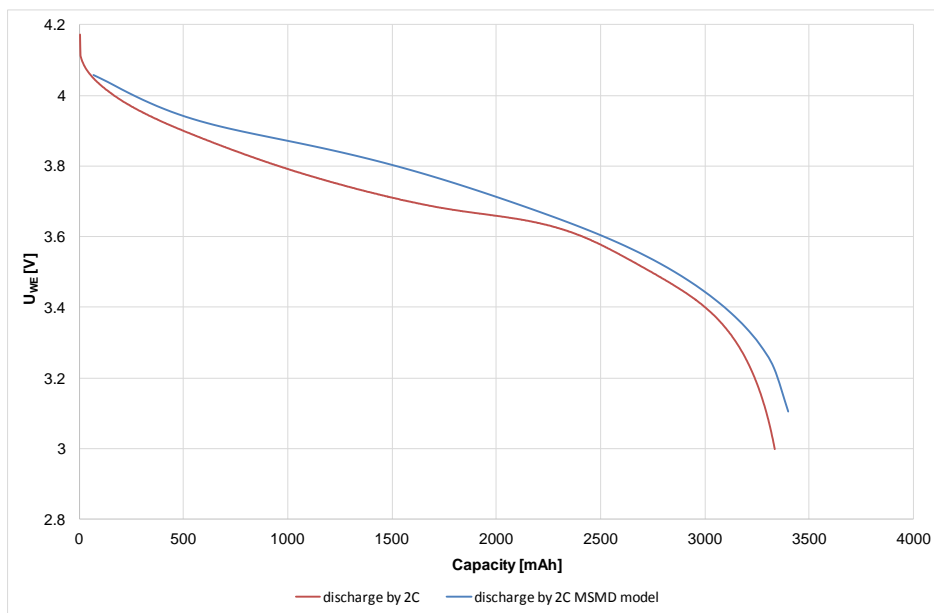


Figure 6. Comparison of the discharge curves at 2 C discharge current for the real KOKAM battery (red) and the mathematical physical model KOKAM (blue)

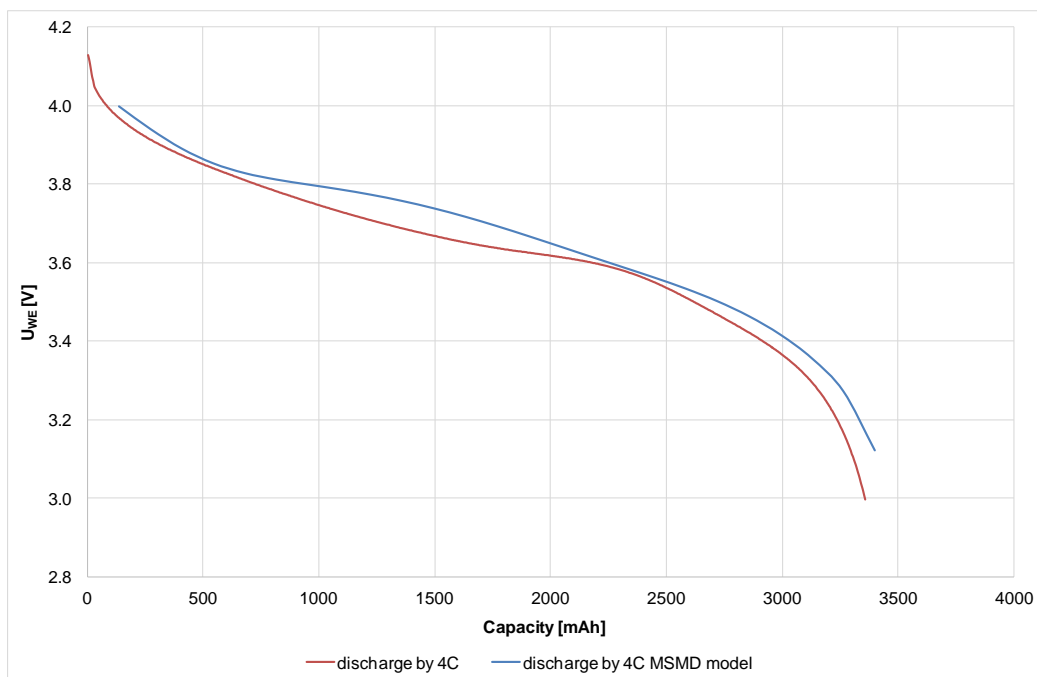


Figure 7. Comparison of the discharge curves at 4 C for the real KOKAM battery (red) and the mathematical physical model KOKAM (blue)

The temperature distribution from the measurement and simulation coincide as in the previous case.

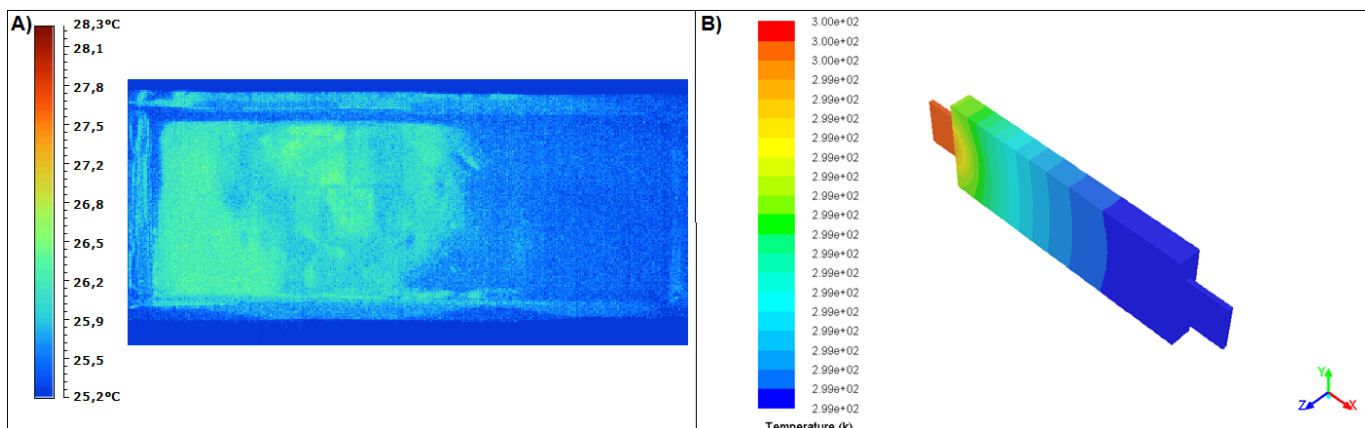


Figure 8. Distribution of temperature field during discharging at 1 C, A) real KOKAM battery; B) mathematical physical model KOKAM

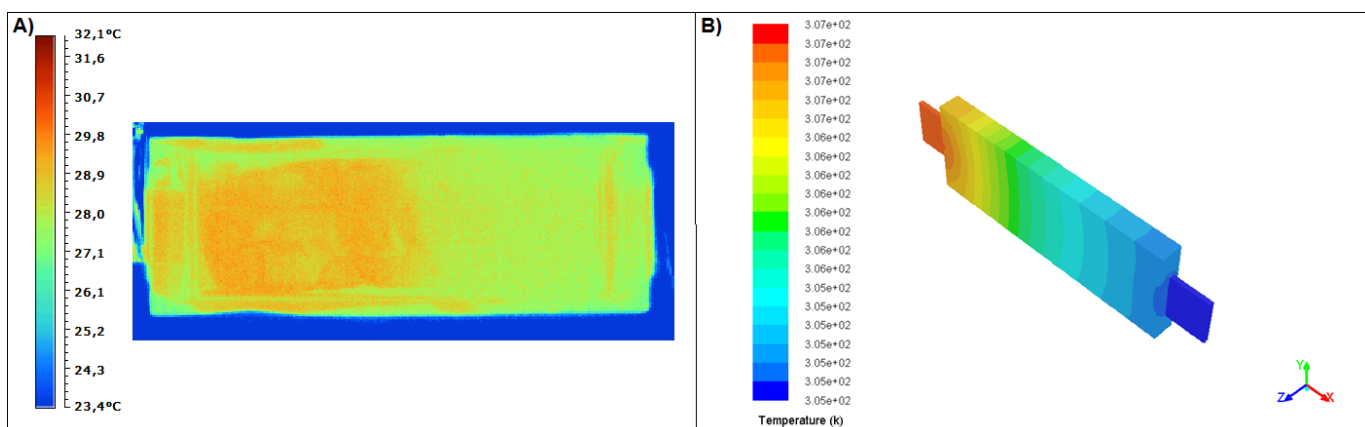


Figure 9. Distribution of temperature field during discharging at 2 C, A) real KOKAM battery; B) mathematical physical model KOKAM

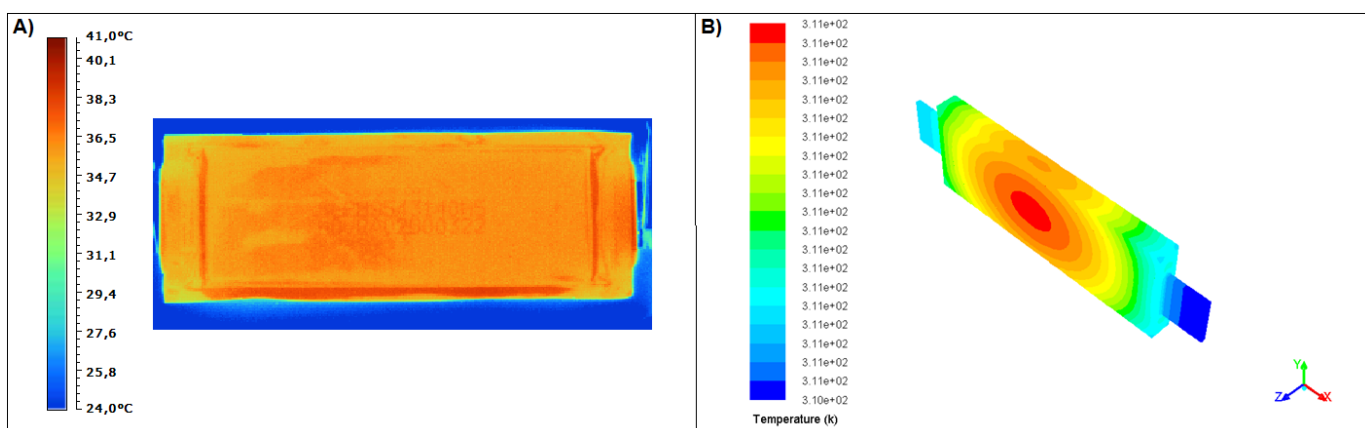


Figure 10. Distribution of temperature field during discharging at 4 C, A) real KOKAM battery; B) mathematical physical model KOKAM

We can see from table 2 that the difference between the maximal measured temperature (32.1 °C) and maximal temperature from the simulation (33.83 °C) is 5.3 %. The last measurement of temperature during discharging was carried out at the current load of 4 C (Fig. 10). Once again, we see that the temperature distribution for the simulation and measurements are identical.

The difference between the observed maximum temperatures is very small; it was 40.0 °C during the measurement and 40.56 °C in the case of simulation, which corresponds to the difference of 1.7 %. These temperatures are very low in comparison with the temperatures that were observed by measurements and simulations in cylindrical batteries. Temperatures reported in the articles for cylindrical batteries at 1 C were around 40 °C and at 4 C about 60 °C.[16, 17] This difference stems from the difference in the construction of the battery. It was found that for a similar type of pouch battery with 40 Ah capacity discharged by 1 C the temperature was around 31 °C and at 2 C about 36 °C which are slightly higher temperatures than the temperatures observed in this article by measurement and simulation. [18]

Table II. Comparison of the real temperatures reached during discharging and temperatures obtained by the simulation

| Discharge current [A] | Measured maximum temperature [°C] | Calculated maximum temperature [°C] | Relative error [%] |
|------------------------------|--|--|---------------------------|
| 1C | 28.30 | 26.95 | 4,70 |
| 2C | 32.10 | 33.83 | 5.30 |
| 4C | 41.00 | 40.56 | 1.07 |

5. CONCLUSION

Higher level domain does not require resolving lower level geometry. Electrode domain does not need to capture the particle geometry. Cell domain does not need to conform or capture the electrode layers. Multi-Scale Multi-Domain model provides a significant flexibility for the cell domain modeling. The software structure is easy to maintain and allows for various sub-models. The advantage of Multi-Scale Multi-Domain numerical model is a relatively high calculation speed, which ranges in the order of minutes with relatively accurate results. The quality of the computational mesh has the greatest influence on the actual computational time. The simulation will be more accurate if the computational mesh is finer and better quality. It implies from the results that the used model is sufficiently accurate. It holds for both capacity testing, where the deviation from the real measurement was about 3 %, and the distribution of the temperature, where the maximal deviation was 5.3 %. It was thus possible to predict the behavior of the accumulator at extreme current rates or, in the next step, at higher ambient temperature. These possibilities would make testing of these accumulators significantly easier.

ACKNOWLEDGEMENTS

This research work has been carried out in the Centre for Research and Utilization of Renewable Energy (CVVOZE). Authors gratefully acknowledge financial support from the Ministry of Education, Youth and Sports of the Czech Republic under NPU I programme (project No. LO1210).

References

1. D. Linden and T. B. Reddy, *Handbook of Batteries*, McGraw-Hill, Michigan (2002).
2. N. Nitta, F. Wu, J. T. Lee, G. Yushin, *Materials Today*, 18 (2015) 252.
3. B. Scrosati, *J Solid State Electrochem*, 15 (2011) 1623.
4. M. S. Whittingham, *Chemical reviews*, 104 (2004) 4271.
5. R. J. Brodd and M. Doeff, in *Batteries for Sustainability*, p. 5, Springer New York.
6. N. Williard, W. He, C. Hendricks and M. Pecht, *Energies*, 6 (2013) 4682.
7. H. D. Yoo, E. Markevich, G. Salitra, D. Sharon and D. Aurbach, *Materials Today*, 17 (2014) 110.
8. P. Vybroubal, J. Maxa, T. Kazda, and J. Vondrak, *ECS Transactions*, 48 (2014) 289.
9. K. H. Kwon, C. B. Shin, T. H. Kang and C.-S. Kim, *Journal of Power Sources*, 163 (2006) 151.
10. U. S. Kim, J. Yi, C. B. Shin, T. Han and S. Park, *Journal of The Electrochemical Society*, 158 (2011) A611.
11. U. S. Kim, C. B. Shin and C.-S. Kim, *Journal of Power Sources*, 180 (2008) 909.
12. Kokam SLPB9543140H5 technical specification.
13. V. Muenzel, A. F. Hollenkamp, A. I. Bhatt, J. de Hoog, M. Brazil, D. A. Thomas and I. Mareels, *Journal of The Electrochemical Society*, 162 (2015) A1592.
14. M. Dubarry and B. Y. Liaw, *Journal of Power Sources*, 194 (2009) 541.
15. S. X. Chen, K. J. Tseng and S. S. Choi, *Power and Energy Engineering Conference, 2009 APPEEC 2009. Asia-Pacific*, p. 1 (2009).
16. D. H. Jeon and S. M. Baek, *Energy Conversion and Management*, 52 (2002) 2973.
17. S. Al-Hallaj and J. R. Selman, *Journal of Power Sources*, 110 (2002) 341.
18. M. Dubarry and B. Y. Liaw, *Journal of Power Sources*, 194 (2009) 541.

© 2016 The Authors. Published by ESG (www.electrochemsci.org). This article is an open access article distributed under the terms and conditions of the Creative Commons Attribution license (<http://creativecommons.org/licenses/by/4.0/>).